








Article

The Key Role of Wettability and Boundary Layer in Dissolution Rate Test

Alice Biasin ¹, Federico Pribac ¹, Erica Franceschinis ², Angelo Cortesi ¹, Lucia Grassi ¹, Dario Voinovich ³, Italo Colombo ¹, Gabriele Grassi ⁴, Gesmi Milcovich ^{5,6,*}, Mario Grassi ^{1,*} and Michela Abrami ¹

- ¹ Department of Engineering and Architecture, University of Trieste, Via Valerio 6/A, I-34127 Trieste, Italy; alice.biasin@phd.units.it (A.B.); federico.pribac@studenti.units.it (F.P.); angelo.cortesi@dia.units.it (A.C.); lucia.grassi@studenti.units.it (L.G.); italo.colombo@protonmail.com (I.C.); michela.abrami@dia.units.it (M.A.)
- ² Department of Pharmaceutical and Pharmacological Sciences, University of Padova, Via Marzolo 5, I-35131 Padova, Italy; erica.franceschinis@unipd.it
- ³ Department of Chemical and Pharmaceutical Sciences, University of Trieste, Via Giorgeri 1, I-34127 Trieste, Italy; vojnovic@units.it
- ⁴ Clinical Department of Medical, Surgical and Health Sciences, Cattinara University Hospital, Trieste University, Strada di Fiume 447, I-34149 Trieste, Italy; ggrassi@units.it
- ⁵ Department of Biological, Chemical and Pharmaceutical Sciences and Technologies, University of Palermo, I-90128 Palermo, Italy
- ⁶ Department of Life Sciences, University of Modena and Reggio Emilia, I-41125 Modena, Italy
- * Correspondence: gesmi.milcovich@unimore.it (G.M.); mario.grassi@dia.units.it (M.G.)

Abstract: Background/Objectives: The present work proposes a mathematical model able to describe the dissolution of poly-disperse drug spherical particles in a solution (Dissolution Rate Test—DRT). DRT is a pivotal test performed in the pharmaceutical field to qualitatively assess drug bioavailability. Methods: The proposed mathematical model relies on the key hallmarks of DRT, such as particle size distribution, solubility, wettability, hydrodynamic conditions in the dissolving liquid of finite dimensions, and possible re-crystallization during the dissolution process. The spherical shape of the drug particles was the only cue simplification applied. Two model drugs were considered to check model robustness: theophylline (both soluble and wettable) and praziquantel (both poorly soluble and wettable). Results: The DRT data analysis within the proposed model allows us to understand that for theophylline, the main resistance to dissolution is due to the boundary layer surrounding drug particles, whereas wettability plays a negligible role. Conversely, the effect of low wettability cannot be neglected for praziquantel. These results are validated by the determination of drug wettability performed while measuring the solid–liquid contact angle on four liquids with decreasing polarities. Moreover, the percentage of drug polarity was determined. Conclusions: The proposed mathematical model confirms the importance of the different physical phenomena leading the dissolution of poly-disperse solid drug particles in a solution. Although a comprehensive mathematical model was proposed and applied, the DRT data of theophylline and praziquantel was successfully fitted by means of just two fitting parameters.

Keywords: DRT; dissolution; particles; wettability; hydrodynamics; mathematical modelling



Citation: Biasin, A.; Pribac, F.; Franceschinis, E.; Cortesi, A.; Grassi, L.; Voinovich, D.; Colombo, I.; Grassi, G.; Milcovich, G.; Grassi, M.; et al. The Key Role of Wettability and Boundary Layer in Dissolution Rate Test. *Pharmaceutics* **2024**, *16*, 1335. <https://doi.org/10.3390/pharmaceutics16101335>

Academic Editor: Peter Timmins

Received: 3 September 2024

Revised: 10 October 2024

Accepted: 14 October 2024

Published: 18 October 2024



Copyright: © 2024 by the authors. Licensee MDPI, Basel, Switzerland. This article is an open access article distributed under the terms and conditions of the Creative Commons Attribution (CC BY) license (<https://creativecommons.org/licenses/by/4.0/>).

1. Introduction

DRT (Dissolution Rate Test) is an essential test, widely used in the pharmaceutical field, that involves the dissolution of different solid poly-disperse drug particles within a liquid environment, mainly water or a physiological fluid [1,2]. This is a key drug hallmark, which is strictly connected to its main properties, such as drug solubility, wettability, and particles' shape and related size distribution. Considering that bioavailability depends on both drug permeability through the cell membrane and drug dissolution properties in physiological fluids [3], DRT can represent a qualitative approach to assess drug bioavailability. Indeed, the drug is absorbed to an extent and rate, becoming available on the site of

drug action [3,4]. This is of pivotal importance: about 40% of the drugs currently on the market and 70–90% of new chemical entities are characterized by low dissolution kinetics due to their poor water solubility [4–8]. Therefore, DRT, correlating with the *in vivo* drug dissolution behavior, represents a key tool in the effective development of pharmaceutical products. For these reasons, drug dissolution profiles and DRT have drawn the attention of many researchers. Hixson and Crowell pioneered the core subject back in 1931 [9–11], considering for the first time the effect of surface reduction following the dissolution of spherical particles and established the cubic law. Later on, Niebergall and co-workers [12] observed a deviation from the cubic law and proposed an improvement, assuming that the thickness of the diffusion layer surrounding the dissolving particle was proportional to the square root of the mean particle diameter. The elegant approach of Pedersen and co-workers extended the mathematical modelling of dissolution to poly-disperse spherical particles [13–16]. Remarkably, this model reduces to the Hixson–Crowell model in monodisperse system models. Other authors stated that the overall dissolution process can be affected by the occurrence of a surface reaction [17] between solute and solvent molecules or by limited solid surface wettability [18]. Regardless of the mechanisms, the final result is a time-dependent drug concentration at the solid–liquid interface that is lower than the drug solubility in the solvent. A similar phenomenon pertains to metastable solids undergoing a phase change (amorphous–crystalline or polymorphic transformation) during the dissolution process, resulting in a time-dependent solid drug solubility [19,20]. Interestingly, the possible drug degradation in the bulk fluid after dissolution was also considered [21]. Of course, researchers focused on the effect of particles shape on dissolution as well [22]. While Hirai and co-workers did not explicitly consider the shape of the particles, they proposed a law that can describe the dissolution surface in a time-dependent fashion [23]. Abrami et al. dealt with spherical, cylindrical, and parallelepiped particles [20]. Hsu and Wu [24] considered sphere-, cylinder-, bi-cone-, cone-, and inverse-cone-shaped particles, whereas Yuan and co-workers focused on the dissolution of irregularly shaped particles [25]. Therefore, particle shape is connected with two additional core dissolution features, i.e., drug concentration profile in the boundary layer (BL) surrounding the solid surface and BL thickness. Indeed, it can be demonstrated that drug concentration profile is not linear, as originally assumed [26–29], unless dissolution occurs from a flat surface. Moreover, BL thickness depends both on dissolution medium hydrodynamic conditions and particle dimension, as documented by D’Arcy and Persoons [30,31]. Recently, Abrami and co-workers gathered most of the parameters correlated with dissolution in an effective mathematical model [32]. They focused mainly on particle shape, specifically on the local surface curvature radius, describing the dissolution both from concave and convex surfaces. Hence, the dissolution of solid particles of any shape can be considered.

Therefore, this work aims to elucidate a tricky, still-pivotal issue: the combined effect exerted on DRT kinetics both by the boundary layer surrounding each drug particle and the drug wettability. At this purpose, the DRT profiles of two different model drugs (theophylline, TPH—good solubility and wettability—and praziquantel, PRQ—poor solubility and wettability) were studied. Indeed, a mathematical model was proposed, with the core phenomena involved as the dissolution of polydisperse particles. Herein, it is hypothesized that the model relies on the immediate attainment of pseudo-stationary conditions, which concern drug mass transport inside the boundary layer. Despite the general complexity of the developed mathematical model, its numerical solution and its data fitting to experimental data were realized within a Microsoft Excel sheet as a user-defined function. This proposes the model as very user-friendly and, thus, targeted to a broad audience plethora, as its application is suitable also for researchers not generally used to dealing with mathematical models. Moreover, the simple solution strategy proposed fosters an approach particularly suited for an industrial environment, too. Herein, rapid and precise answers are usually needed. Hence, it is very important to understand the relative importance of different phenomena in order to improve the performance of drug delivery systems.

2. Materials and Methods

2.1. Drugs

The first model drug considered was theophylline (TPH), a bronco-dilatator indicated for the treatment of asthma, bronchospasm, and Chronic Obstruction Pulmonary Diseases (COPD) (Carlo Erba, Milano, Italy; $C_7H_8N_4O_2 \cdot H_2O$, Mw = 198.2; essentially a neutral compound characterized by water solubility of 12,495 $\mu\text{g}/\text{mL}$ at 37 °C and maximum UV absorbance at wavelength 272 nm [33]). The second model drug was praziquantel (PRQ), used to treat the infections of different parasites, such as schistosomiasis (kind gift by Fatro S.p.A., Bologna, Italy. $C_{19}H_{24}N_2O_2$, Mw = 312.4; water solubility 180 $\mu\text{g}/\text{mL}$ at 37 °C and maximum UV absorbance at wavelength 262.6 nm [34,35]).

2.2. Wettability

Drugs wettability was evaluated at 25 °C by measuring the liquid–solid contact angles of four liquids (deionized water (H_2O), formamide (CH_3NO), dimethyl sulfoxide ($(CH_3)_2SO$), and diiodomethane (CH_2I_2), (Sigma-Aldrich, Milano, Italy)) on compacted drug powder measured on a DSA 10 tensiometer (Krüss, Hamburg, Germany) connected to the DSA 4 software (Krüss, Germany). For this purpose, ca. 200 mg of each drug were compressed using a single punch tablet machine (Cosalt, Officina CO.STA, Gorgo al Monticano, Italy) equipped with a 10 mm flat punch. The liquid drop spreading onto the tablets' surface was recorded using the fast digital camera of the tensiometer. The videos were processed by means of the instrument software, and the contact angle (θ) was evaluated by applying the tangent method (T-1) to the image where the base diameter did not increase [36]. Each measurement was performed in triplicate and is reported in Table 1 as mean value \pm standard deviation.

Table 1. Solid–liquid contact angle (θ) referring to TPH and PRQ (25 °C).

Liquid	θ_{TPH}	θ_{PRQ}
H_2O	49 ± 2.1	71.6 ± 1.3
CH_3NO	20.5 ± 4.1	41.6 ± 7.6
$(CH_3)_2SO$	14.4 ± 2.2	25.7 ± 3.0
CH_2I_2	41.4 ± 1.2	18.0 ± 2.3

Based on the contact angle measurements, drug wettability was estimated according to the spreading coefficient S_C defined by the following [37]:

$$S_C = \gamma_{lv}(\cos(\theta) - 1) \quad (1)$$

where θ is the solid–liquid contact angle while γ_{lv} is the liquid–vapor surface energy that, for the four liquids considered, is reported in Table 2, as well as the polar and dispersion components [18]. The data reported in Tables 1 and 2 allow us to evaluate the polarity of the model drug considered, following the Wu approach [38]. According to this approach, the solid–vapor surface energy (γ_{sv}) is the sum of a polar (γ_{sv}^P) and a dispersion component (γ_{sv}^d). The two γ_{sv} components can be evaluated by the simultaneous solution of the following system of nonlinear equations:

$$\begin{cases} \gamma_{1lv}(1 + \cos \theta_1) = \frac{4\gamma_{sv}^d \gamma_{1lv}^d}{\gamma_{sv}^d + \gamma_{1lv}^d} + \frac{4\gamma_{sv}^P \gamma_{1lv}^P}{\gamma_{sv}^P + \gamma_{1lv}^P} \\ \gamma_{2lv}(1 + \cos \theta_2) = \frac{4\gamma_{sv}^d \gamma_{2lv}^d}{\gamma_{sv}^d + \gamma_{2lv}^d} + \frac{4\gamma_{sv}^P \gamma_{2lv}^P}{\gamma_{sv}^P + \gamma_{2lv}^P} \end{cases} \quad (2)$$

where θ_1 and θ_2 are the contact angles referring to a polar (water) and a non-polar (diiodomethane) fluid, respectively (Table 1), γ_{1lv} and γ_{2lv} are the liquid–vapor surface energies referring to the two liquids, and γ_{1lv}^P , γ_{2lv}^P , γ_{1lv}^d , and γ_{2lv}^d are, respectively, their polar and dispersion components reported in Table 2. The solution of the equation system is reported in Table 3. In order to confirm the Wu approach, γ_{sv} was evaluated according to

the state equation approach proposed by Kwok, Neumann, and Li [39,40] as per all the four contact angles shown in Table 1. This check supported the Wu approach, as we detected γ_{sv} (mJ/m²) = 61 (TPH) and γ_{sv} (mJ/m²) = 47 (PRQ).

Table 2. Liquid–vapor surface energy (γ_{lv}) and relative polar (γ_{lv}^p) and dispersion (γ_{lv}^d) components (25 °C) [18].

Liquid	γ_{lv} (mJ/m ²)	γ_{lv}^p (mJ/m ²)	γ_{lv}^d (mJ/m ²)	Polarity%
H ₂ O	71.8	51.0	21.8	70.0
CH ₃ NO	68.0	19.0	39.0	32.7
(CH ₃) ₂ SO	44.0	8.0	36.0	18.2
CH ₂ I ₂	50.8	6.7	44.1	13.2

Table 3. Solid–vapor surface energy (γ_{sv}) and relative polar (γ_{sv}^p) and dispersion (γ_{sv}^d) components evaluated according to the Wu approach.

Drug	γ_{sv} (mJ/m ²)	γ_{sv}^p (mJ/m ²)	γ_{sv}^d (mJ/m ²)	Polarity%
Theophylline	55.1	27.8	27.2	50.6
Praziquantel	50.6	38.0	12.6	24.9

2.3. Particle Size

The particle size distribution (PSD) of TPH and PRQ powders was evaluated by Dynamic Laser Light Scattering (Mastersizer Hydro 2000, Malvern Instruments, Malvern, UK) using as a dispersant liquid silicone oil (cyclomethicone K4, ACEF, Fiorenzuola d'Arda, Italy) for theophylline and deionized water plus 1% (*w/w*) polysorbate 80 (ACEF, Italy) for praziquantel.

Powders were dispersed in a small amount of dispersant. The suspensions were mixed by magnetic stirring and then added to the instrument's dispersion unit, containing about 200 mL of dispersing liquid, until the quenching reached a value between 10% and 20%. The analysis was performed in triplicate, using a dispersion unit controller set to 1800 rpm.

Particle size distributions were calculated according to Mie theory [41] by means of the following refractive index values: 1.330 for silicone oil, 1.360 for water, and 1.700 for theophylline and praziquantel. For mathematical modeling purposes, we hypothesized that particles were spherical. The cumulative PSDs referring to the TPH and PRQ are reported in Figure 1.

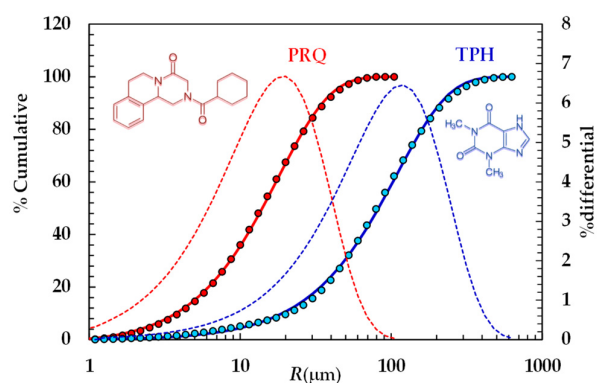


Figure 1. Particle size distribution referring to TPH and PRQ (symbols). Continuous lines indicate the best fitting of the cumulative Weibull distribution (Equation (3)), while dotted lines indicate the differential particle size distribution (right vertical axis).

In the light of the mathematical model proposed to study DRT, the Weibull distribution [42] was fitted to the experimental PSD referring to the two model drugs considered:

$$W\% = 100 \times \left(1 - e^{-\left(2\frac{R-R_{\min}}{\phi}\right)^\varphi}\right) \quad (3)$$

The values of the fitting parameters jointly with the average radius (R_A) are reported in Table 4.

Table 4. Fitting parameters of the Weibull distribution (Equation (3)) referring to the two model drugs considered. R_A is the average radius of the distribution.

Drug	R_{\min} (μm)	ϕ (μm)	φ (-)	R_A (μm)
Theophylline	0.48	218.9	1.266	109.6
Praziquantel	0.79	35.3	1.256	18.5

2.4. DRT Test

A pre-determined amount of drug (3 mg TPH; 27 mg PRQ) was dispersed in 150 mL of distilled-degassed water contained in a proper thermostatic glass vessel (37 °C). As both PRQ solubility and molar extinction (ϵ) are very low, it was necessary to consider a high amount of this drug to be able to check and record the beginning part of the DRT process. On the other hand, TPH did not show this problem, and hence a smaller amount could be considered in the DRT experiments. A magnetic stirrer, lying on the vessel bottom and rotating at 370 rpm, ensured fluid mixing. Drug concentration in the dissolution environment was measured by an optical fiber (HELLMA, Milano, Italy) ending with a probe characterized by an optical path of 5 mm (TPH) or 10 mm (PRQ). With this setup, absorbance was always ≤ 1 . Probe distance from the stirrer was about 5 cm to prevent bubble adhesion on it. The optical fiber was connected to a UV spectrophotometer (ZEISS, MCS 600, Oberkochen, Germany) to record absorbance. In order to avoid the scattering effect of solid particles, the absorbance determined at each drug wavelength (272 nm TPH; 262.6 nm PRQ) was deprived by the absorbance recorded at 500 nm (i.e., very far from the drug wavelength). Indeed, the effect of solid particle scattering is the same whatever the wavelength. Absorbance (ABS) recording started just after drug dispersion in the dissolving medium. Molar extinction (ϵ) of TPH and PRQ were 12,117 ($\text{M}^{-1} \times \text{cm}^{-1}$) and 342.3 ($\text{M}^{-1} \times \text{cm}^{-1}$), respectively (see Appendix A). All tests were performed in triplicate.

3. Mathematical Modelling

The dissolution phenomenon of a solid in a liquid environment is associated with four steps that can be seen as energetic barriers, hindering the dissolution process [20]. These refer to (1) contact of the solvent with the solid surface (wetting; ΔE_w), (2) breakdown of intermolecular bonds in the solid phase (fusion; ΔE_f), (3) molecules' transfer from the solid phase to the solid-liquid interface (solvation; ΔE_s), (4) diffusion of the solvated molecules through the unstirred boundary layer (BL) surrounding the solid surface (diffusion; ΔE_d) (see Figure 2). These steps represent the total resistance for the drug molecules' movement from the solid phase to the solution one (dissolution). Moreover, the first three steps are connected to the surface resistance (R_m) for drug dissolution, while the last one ($R_d = \delta/D$) represents the drug resistance to cross the BL of thickness (d) and drug diffusivity D (see Figure 2). Indeed, R_d is connected to the hydrodynamic conditions of the liquid environment. As the present work aims to model the dissolution from different poly-disperse spherical drug particles, it is necessary to consider the contribution to dissolution due to each one (ith class) of the N dimensional classes, into where the continuous particle size distribution can be split. Indeed, dissolution kinetics depends on particle radius. Thus, from now on, we will focus on the development of our model, drawing attention to the ith class.

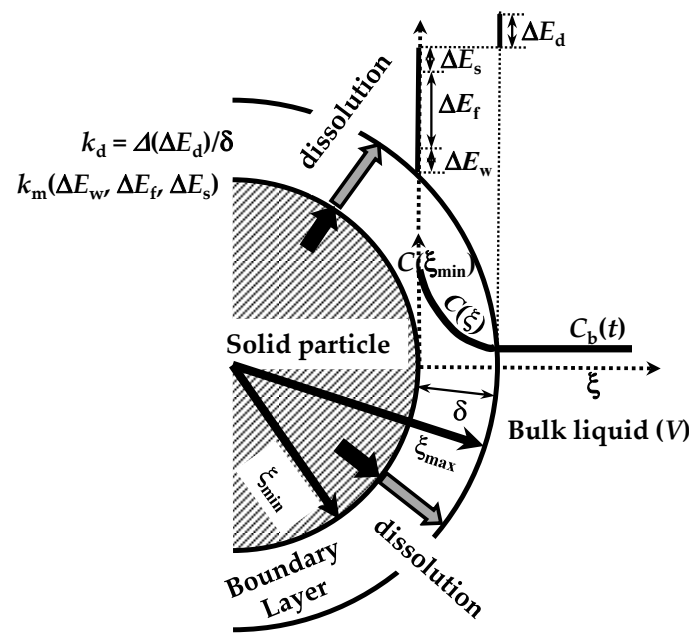


Figure 2. Four energetic barriers hinder the dissolution of a solid drug in a solvent: solid wetting (ΔE_w), breakdown (fusion) of solid molecular bonds (ΔE_f), drug molecules' solvation (ΔE_s), and drug molecules' diffusion through the boundary layer surrounding the solid particle (ΔE_d). These energies affect, in different manners, the mass transfer coefficient (k_m) at the solid–liquid interface and the dissolution constant k_d . Notably, due to possible solid surface wetting problems, the drug molecule concentration at the solid–liquid interface ($C(\xi_{\min})$) can be lower than drug solubility in the dissolution medium. ξ indicates the radial coordinate while V is the dissolution environment volume. Adapted from [28].

Fick's second law represents the starting point to blend the four dissolution steps. Herein, it is hypothesized that pseudo-stationary conditions hold within the BL, so that Fick's second law reads as follows [32]:

$$\nabla(D\nabla C_i) = 0 \quad (4)$$

where C_i is the position-dependent drug concentration inside the BL of the i th class. Assuming that mass transport essentially occurs in the radial direction (ξ^i), Equation (4) must be solved according to the following boundary conditions:

$$(D\nabla C_i \cdot \mathbf{n}_i)|_{\xi^i = \xi_{\min}^i} = -k_m(C_s - C(\xi_{\min}^i)) \quad (5)$$

$$C(\xi_{\max}^i) = C_b \quad (6)$$

where ξ_{\max}^i and ξ_{\min}^i are the radii defining the BL thickness δ_i (see Figure 2), C_s is the drug solubility in the dissolution medium, \mathbf{n}_i is the normal vector to the particle surface, C_b is the time-dependent drug concentration in the dissolution medium, and k_m is the mass transfer coefficient related to the first three steps of the dissolution process and mainly depending on the surface wettability.

Equation (5) requires that the drug flux leaving the solid surface is driven by both k_m and the difference between C_s and the drug concentration at the solid–liquid interface ($\xi^i = \xi_{\min}^i$). Equation (6) states that the drug concentration at the BL-dissolution medium ($\xi^i = \xi_{\max}^i$) is equal to the bulk concentration C_b .

Although k_m depends on the surface curvature radius (ξ_{\min}^i), thus it should be class-dependent (k_m^i), this dependence is so small that it can be neglected and k_m can be assumed constant for every N class [32]. Conversely, the drug resistance, $R_d^i = \delta_i/D$, due to the drug

crossing the BL of thickness δ_i and drug diffusion coefficient D (step 4), depends on many physical parameters, such as the particle curvature radius (ζ_{\min}^i). D'Arcy and Persoons nicely modelled this dependence in terms of the hydrodynamics mass transfer coefficient $k_d^i (=1/R_d^i$; also referred to as intrinsic dissolution constant) [30,31]:

$$k_d^i = \frac{D}{2\zeta_{\min}^i} \left(2 + 0.6 \sqrt{\Delta U \frac{2\zeta_{\min}^i}{\nu_f} \left(\frac{\nu_f}{D} \right)^{\frac{1}{3}}} \right) \Delta U = \alpha \frac{(\rho_s - \rho_f)}{\rho_f} g \frac{(2\zeta_{\min}^i)^2}{18\nu_f} \quad (7)$$

where ρ_s and ρ_f are, respectively, the solid drug and the fluid density, ν_f is the fluid kinematic viscosity, g is the gravity acceleration, ΔU is the absolute relative velocity between particles and fluid, and α is an adjustable parameter (≥ 0), which was set to 1 on the original D'Arcy and Persoons model.

Equation (4)'s analytical solution, in the light of boundary conditions (Equations (5) and (6)), reads as follows:

$$C_i(\zeta^i) = C_b + (C_s - C_b) \frac{\frac{k_m}{k_d^i} (\zeta_{\min}^i)^2 \left(\frac{k_d^i}{D} \left(\frac{\zeta_{\min}^i}{\zeta^i} - 1 \right) + \frac{1}{\zeta^i} \right)}{\zeta_{\min}^i \left(1 + \frac{k_m}{k_d^i} \right) + \frac{D}{k_d^i}} \quad (8)$$

Equation (8) clearly shows that drug concentration inside BL is not linearly dependent on the radial position ζ^i . Based on Equation (8) it is possible to determine the drug concentration at the solid drug–BL interface ($C_0^i = C(\zeta_{\min}^i)$):

$$C_0^i = C_b + (C_s - C_b) \frac{\zeta_{\min}^i}{\frac{k_d^i}{k_m} \zeta_{\max}^i + \zeta_{\min}^i} \quad (9)$$

Equation (9) states that C_0^i is always less than C_s and it equates C_s only when $C_b = C_s$, i.e., after a very long time and when the solid drug amount is sufficient to obtain C_s in the dissolution environment. Clearly, when k_m is very large (i.e., the mass transfer resistance $R_m = 1/k_m$ is vanishing), C_0^i immediately equates C_s . On the contrary, when surface wettability is very poor, k_m is very small (i.e., the mass transfer resistance $R_m = 1/k_m$ is very big) and C_0^i is very close to C_b so that dissolution kinetics will be very slow.

As it is quite common that, during the dissolution process, the drug undergoes a phase transformation (polymorphic or amorphous–crystalline), drug solubility can reduce over time. This phenomenon is usually described by a first order reaction [43] occurring at the solid–liquid interface and leading to the following expression for the C_s temporal reduction:

$$C_s = C_{sf} + (C_{s-in} - C_{sf}) e^{(-k_r t)} \quad (10)$$

where C_{sf} and C_{s-in} are, respectively, the final and initial values of solubility, while k_r is the recrystallization constant and t is time. Indeed, Equation (10) refers to the dissolution step 2, as solubility is directly connected with the crystal network breakdown attitude, quantified by its melting temperature and enthalpy [44].

In order to evaluate the particles' radii (ζ_{\min}^i) time decrease, it is necessary to consider N ordinary differential equations (one for each class) referring to the particles mass (M_i) reduction:

$$\frac{dM_i}{dt} = \frac{d}{dt} \left(\rho_s \frac{4}{3} \pi \left(\zeta_{\min}^i \right)^3 \right) = 4\pi \left(\zeta_{\max}^i \right)^2 \left(D \frac{\partial C_i}{\partial \zeta^i} \right) \Big|_{\zeta^i = \zeta_{\max}^i} \quad (11)$$

Equation (11) states that the time reduction of the i th particle mass equates the mass amount leaving the particle through the surface located at the end of the BL ($\zeta^i = \zeta_{\max}^i$). As Equation (8) allows us to evaluate the partial derivative appearing in Equation (11),

after some algebraic manipulations, Equation (11) can be re-written in a simpler and more straightforward form:

$$\frac{d\zeta_{\min}^i}{dt} = \frac{K_i}{\rho_s} (C_s - C_b) \quad K_i = \frac{\zeta_{\min}^i / \zeta_{\max}^i}{\left(\frac{1}{k_d^i} + \frac{1}{k_m} \left(\frac{\zeta_{\max}^i}{\zeta_{\min}^i}\right)\right)} \quad (12)$$

where K_i is the overall mass transport coefficient referred to both k_d^i and k_m . Its inverse represents the global mass transport resistance (R_i), sum of R_m and R_d^i . Obviously, Equation (12) works only when $C_b < C_s$, i.e., when particle dissolution can take place. When the above mentioned condition does not take place, ξ^i would be constant, as its time derivative would be zero (second right term of Equation (12)). In this case, part of the already dissolved drug inside the dissolution medium would precipitate, and this phenomenon can be modelled as per the following first order equation:

$$\frac{dM_c}{dt} = k_{rb} V (C_s(t) - C_b(t)) \quad (13)$$

where M_c is the amount of re-crystallized drug ($M_c = 0$ at the beginning of the dissolution process), V is the dissolution volume, and k_{rb} is the bulk re-crystallization constant, which is usually assumed to be equal to k_r [20] (see Equation (10)). In order to balance unknowns and equations, it is possible to refer to an overall mass balance, where, at any time, the initial solid mass (M_0) must be equal to the sum of the undissolved drug mass, the solubilized drug present in the bulk solution, and M_c :

$$M_0 = \sum_{i=1}^{i=N} \rho_s N_{pi} V_{pi} + C_b(t) V + M_c(t) \quad \text{or} \quad C_b(t) = \frac{M_0 - \sum_{i=1}^{i=N} \rho_s N_{pi} V_{pi} - M_c(t)}{V} \quad (14)$$

where N_{pi} indicates the number of particles belonging to the i th class and, thus, sharing the same radius at the beginning of the dissolution process ($\zeta_{\min-0}^i$), which can be deduced from the Weibull equation (Equation (3)) characterizing the particle size distribution:

$$N_{pi} = V_0 \frac{(V_i - V_{i-1})}{\frac{4}{3}\pi(\zeta_{\min-0}^i)^3} \quad V_{pi} = \frac{4}{3}\pi(\zeta_{\min}^i)^3 \quad (15)$$

where V_0 is the particles volume ($=M_0/\rho_s$) while V_i and V_{i-1} are defined by the following:

$$V_i = 1 - e^{-(2\frac{\zeta_{\min}^i - R_{\min}}{\phi})^\varphi} \quad V_{i-1} = 1 - e^{-(2\frac{\zeta_{\min}^{i-1} - R_{\min}}{\phi})^\varphi} \quad (16)$$

where R_{\min} represents the smallest particle's radius at the beginning of the dissolution. The numerical solution of model equations (see Appendix B for details) allows us to determine the time variation of the bulk drug concentration (C_b) as well as the drug concentration inside the BL for each of the N particles classes.

4. Results and Discussion

4.1. Microscopic Results

Before checking the model on the experimental DRT data, it is interesting to look at the microscopic information that it provides: the evolution of the drug concentration profile inside the BL during the dissolution process. Such a feature has never been completely handled by other mathematical models. Therefore, we assume that drug recrystallization does not occur—this would just entangle the analysis, with no specific, useful tool related to the physical considerations investigated herein. Furthermore, a monodisperse particle size distribution is considered (thus, superscript/subscript “ i ” will be cut in this section) and usual values are fixed for the parameters leading the dissolution process (see caption to Figure 3). Equation (8) allows us to draw the variation of the drug concentration profile

inside the BL during the dissolution process. Clearly, C_b^+ (or its dimensionless expression $C_b^+ = C_b/C_s$) is evaluated through the mass balance (Equation (14)), where, based on previous hypotheses, only one class is considered and $M_c = 0$. Moreover, Equation (9) allows us to evaluate the drug concentration at the solid–liquid interface, i.e., in $\xi = \xi_{\min}$. In order to broaden the model applications, dimensionless concentration ($C^+ = C/C_s$) and radial position ($\xi^+ = \xi/\xi_{\min-0}$; $\xi_{\min-0}$ is the initial particle radius) have been set. Figure 3A considers a solid drug that does not show wettability issues, i.e., the k_m/k_d ratio is high (between 10 and 10^2) or, equivalently, the surface resistance $R_m (=1/k_m)$ is small, compared to the hydrodynamic one $R_d (=1/k_d)$. Based on the k_d variation with radius (Equation (7)), a range of k_m/k_d is applied, instead of only one value. The red lines in Figure 3A represent the evolution of the drug concentration profile (Equation (8)) during the dissolution process.

In detail, over Figure 3A, the first red line on the right refers to the drug concentration profile at the beginning ($t = 0$) of the dissolution process. Vertical dashed and dotted lines indicate the dimensionless BL thickness ($\delta^+ = D \times k_d/\xi_{\min-0}$). Thus, the lowermost part of each profile shows the end of the BL ($\xi = \xi_{\max}$), while the uppermost part indicates the beginning of the BL defined by the solid–liquid interface ($\xi = \xi_{\min}$). As the dissolution proceeds, the drug profile concentration moves on the left, as well as particle radius (ξ_{\min}) reducing up to the end of the dissolution (particle disappearing). Furthermore, δ^+ reduces as dissolution proceeds, according to the distance separating dashed or dotted vertical lines. Considering that wettability issues do not occur, the dimensionless drug concentration at the solid–liquid interface (dashed green line, $C^+(\xi_{\min}^+) = C/C_s$) is equal to one, except at the end of the dissolution, when it almost merges to $M_0/(V \times C_s)$, set to 0.625 in our simulations. Thus, drug concentration at the solid–liquid interface is equivalent to drug solubility in the dissolution environment C_s . The blue dashed line represents the trend of the dimensionless drug concentration at the end of the BL, which, according to Equation (6), equals the dimensionless bulk drug concentration C_b^+ . Therefore, C_b^+ starts from zero and terminates at the final value of 0.625 ($=M_0/(V \times C_s)$). When solid wettability decreases (Figure 3B; $0.2 < (k_m/k_d) < 3$), drug concentration at the solid–liquid interface ($\xi = \xi_{\min}$) is never equal to one (see dashed green line), and thus the concentration gradient across the BL is lower, leading to slower dissolution kinetics. Finally, when wettability issues are relevant (Figure 3C), the dimensionless drug concentration at the solid–liquid interface (dashed green line, $C^+(\xi_{\min}^+)$) increases with a monotonic trend from zero up to the final value of 0.625. Therefore, the concentration gradient across BL is fading and the kinetics of the dissolution process are strongly decreased. Overall, the analysis of Figure 3A–C reveals some important theoretical features of the proposed model, i.e., that the evolution of the BL thickness δ^+ is not affected by solid wettability. On the other hand, it influences the drug concentration profile inside BL, hence the drug concentration at the solid–liquid interface ($\xi = \xi_{\min}$).

Remarkably, the C_b^+ evolution (blue dashed lines) is identical for the three wettability conditions examined in Figure 3A–C. This is due to the C_b^+ evolution, which is referred to the reduction of the particle radius and not to time increase. Indeed, the same radius reduction requires an increasing time when drug wettability reduces. Thus, one of the advantages of the proposed model is to provide a kind of analytical solution explaining the evolution of the drug concentration inside BL when a particle dissolves based on a monodisperse distribution (Equations (8) and (9)). Indeed, in order to connect radius reduction to elapsing time, it is required to numerically solve the whole model.

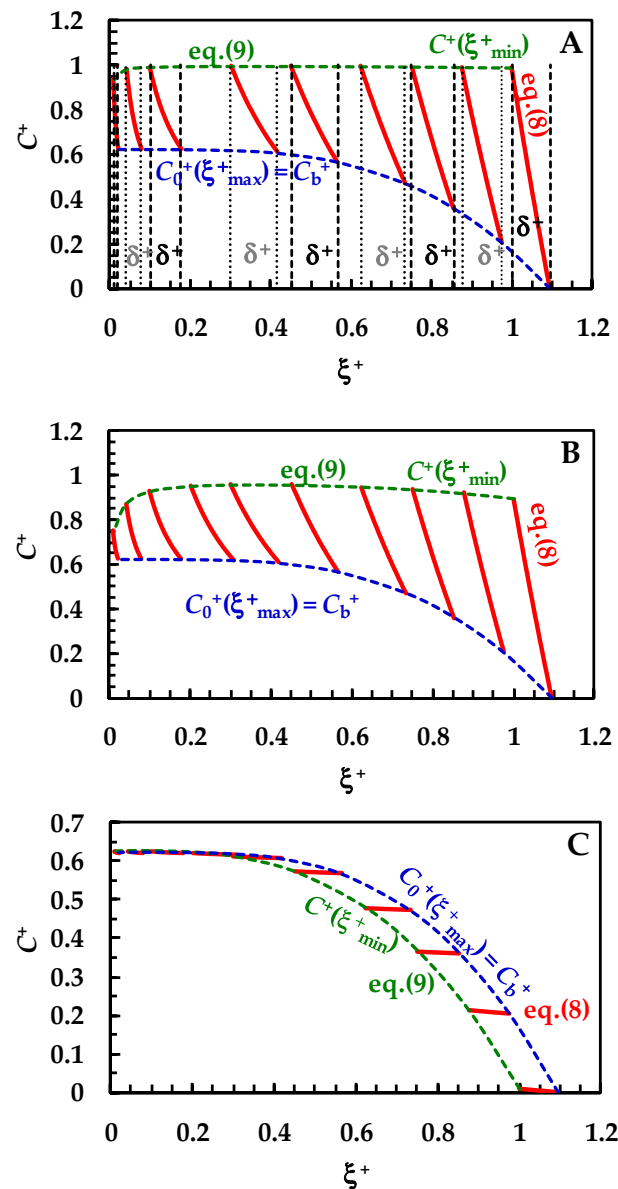


Figure 3. Temporary evolution of the dimensionless drug profile concentration (red lines, Equation (8)) inside BL (ξ^+ is the dimensionless radial coordinate). C_b^+ ($=C_b/C_s$) is the dimensionless drug concentration inside the dissolution medium (dashed blue lines) being C_s drug solubility (assumed constant in time). Dashed green lines (Equation (8)) indicate the dimensionless drug concentration at the solid/liquid interface ($\xi = \xi_{min}$). Three different ranges for the k_m/k_d ratio were considered: (A) $10 < (k_m/k_d) < 10^2$ (no wettability issues). Vertical dashed and dotted lines indicate dimensionless BL thickness δ^+ , (B) $0.2 < (k_m/k_d) < 3$ (moderate wettability issues), and (C) $10^{-3} < (k_m/k_d) < 10^{-2}$ (considerable wettability issues). All other parameters are equal and read as follows: $\rho_s = 1500 \text{ kg/m}^3$, $\rho_f = 1000 \text{ kg/m}^3$, $\eta(\text{Pa s}) = 10^{-3}$, $\nu_f(\text{m}^2/\text{s}) = 10^{-6}$, $D(\text{m}^2/\text{s}) = 10^{-10}$, $C_{inf}/C_s = 0.625$ (C_{inf} is the drug concentration reached in the dissolution medium upon complete dissolution of the solid drug particles), $k_r = 0$, $\alpha = 1$, and $g = 9.81 \text{ m/s}^2$. These values are typical of small organic drugs such as those considered in this work.

4.2. Macroscopic Results: Data Fitting

4.2.1. Theophylline

Figure 4 shows the model's best fitting (solid line) to experimental DRT data (symbols) referring to TPH. In detail, TPH monohydrate is stable in the aqueous dissolution environment. Indeed, it does not undergo re-crystallization upon dissolution. Consequently, the

profile concentration does not show the usual slope reduction at the beginning, induced by the solubility reduction [18]. The data fitting is very accurate, and the values of the two model fitting parameters read $\alpha = 27$ and $k_m = 0.38$ m/s. The fact that α is >1 involves a “disengagement” from the original D’Arcy and Persoons equation for the k_d^i evaluation (Equation (7)). Thus, we conclude that the relative velocity between particles and fluid is greater than that proposed by D’Arcy and Persoons. This is not surprising as their approach, although very useful and smart, represents an approximation of what really occurs between particles and a dissolving fluid. Moreover, it is worth mentioning that their theory refers to spherical particles, while TPH particles appear as solid bodies, i.e., parallelepipeds [20]. The comparison between k_m , k_d^i (Equation (7)) and K_i (Equation (12)), shown in Figure 5, reveals that k_m is $\gg k_d^i$; thus, the overall mass transport coefficient K_i almost matches with k_d^i . Essentially, the most important resistance to TPH dissolution is represented by the existence of the BL surrounding each particle, whose thickness is strictly connected to the hydrodynamic conditions of the dissolution medium. Thus, the analysis of DRT data by means of the proposed model reveals that TPH is not affected by wettability problems.

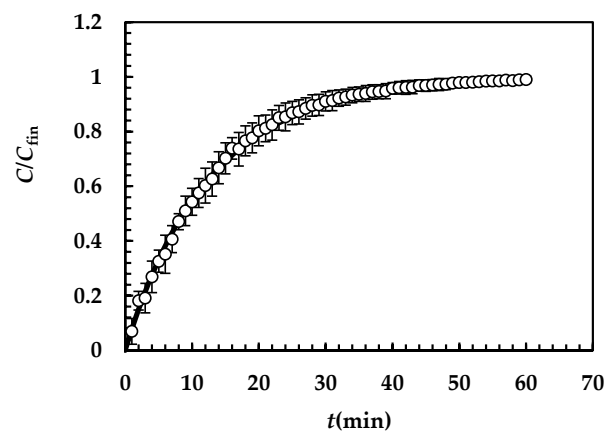


Figure 4. Model’s best fitting (solid line) to experimental DRT data (symbols) referring to TPH (37 °C). Vertical bars indicate data standard error. The physical parameters adopted to perform data fitting read as follows: $\rho_s = 1490$ kg/m³, $\rho_f = 993$ kg/m³, η (Pa s) = 6.91×10^{-3} , ν_f (m²/s) = 0.696×10^{-6} , D (m²/s) = 8.26×10^{-10} , and C_s (kg/m³) = 12.49 [20] while $k_r = k_{rb} = 0$ as monohydrate TPH does not undergo re-crystallization upon dissolution. TPH particle size distribution is described by the Weibull distribution (Equation (3)), whose parameters are those reported in Table 4. Concentration data (C) are normalized with respect to the final concentration $C_{fin} = M_0/V$.

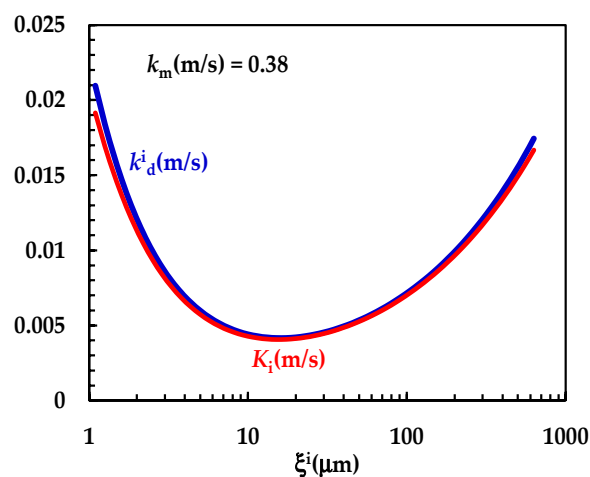


Figure 5. Comparison between k_m and the $k_d^i - K_i$ trend referring to the interpretation of DRT data (TPH) according to the proposed mathematical model.

4.2.2. Praziquantel

Figure 6 reports the model best fitting (solid line) to experimental DRT data (symbols) referring to PRQ. In this situation, no re-crystallization occurs too, as the aqueous dissolution environment did not induce any PRQ structure transformation. Therefore, the profile concentration did not show the usual slope reduction at the beginning due to a solubility reduction [18]. The quality of data fitting is very accurate and the values of the two model fitting parameters read $\alpha = 1$ and $k_m = 0.001$ m/s. Remarkably, for PRQ, α turns out to be equal to one, as assumed by D'Arcy and Persoons (Equation (7)). As the shape of PRQ particles is not too different from that of TPH (PRQ particles resemble needles [34]), we hypothesize that the difference compared to TPH ($\alpha = 27$) is not related to shape. Vice versa, as TPH particles are definitely bigger than the PRQ ones (see Figure 1), α should be mainly affected by particles' dimension.

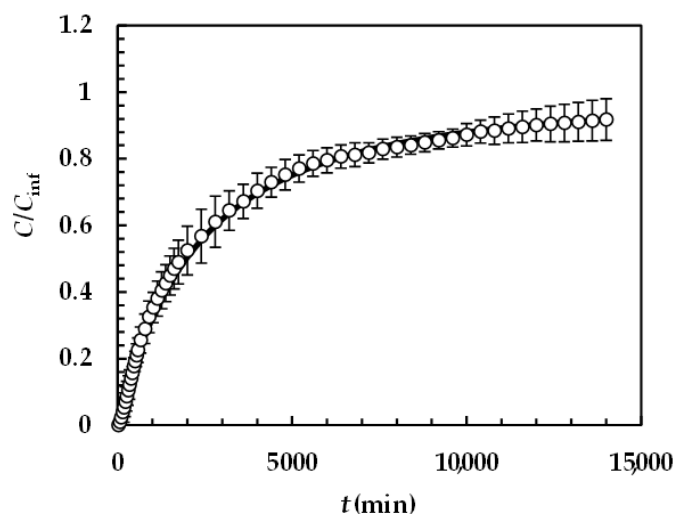


Figure 6. Model's best fitting (solid line) to experimental DRT data (symbols) referring to PRQ (37 °C). Vertical bars indicate data standard error. The physical parameters adopted to perform data fitting read as follows: $\rho_s = 1232$ kg/m³, $\rho_f = 993$ kg/m³, η (Pa s) = 6.91×10^{-3} , ν_f (m²/s) = 0.696×10^{-6} , D (m²/s) = 1.0×10^{-9} , and C_s (kg/m³) = 0.18 [35] while $k_r = k_{rb} = 0$ as PRQ does not undergo re-crystallization upon dissolution. PRQ particle size distribution is described by the Weibull distribution (Equation (3)), the parameters of which are those reported in Table 4. Concentration data (C) are normalized with respect to the final concentration $C_{fin} = M_0/V$.

In order to test this hypothesis, further investigation on the DRT of particles characterized by different shapes and different size distributions is required. The comparison between k_m , k_d^i (Equation (7)) and K_i (Equation (12)) shown in Figure 7 clearly reveals that k_m is comparable with k_d^i (although bigger) and that the overall mass transport coefficient K_i depends on both k_m and k_d^i . The non-negligible contribution to K_i due to k_m demonstrates that $k_d^i > K_i$, as clearly shown in Figure 7. Thus, the mass transfer resistance connected to the PRQ dissolution depends on both the surface ($R_m = 1/k_m = 10^3$ s/m) and the hydrodynamic ($R_d^i = 1/k_d^i \approx 10^3$ – 10^4 s/m) resistances. Therefore, PRQ's slow dissolution kinetics are due to the combination of low solubility and moderate wettability. Indeed, the analysis of DRT data by means of the proposed model allows us to determine and quantify the effect on DRT of some key drug features, such as solubility, wettability, and particles' size distribution. This task would be not easily accomplished otherwise.

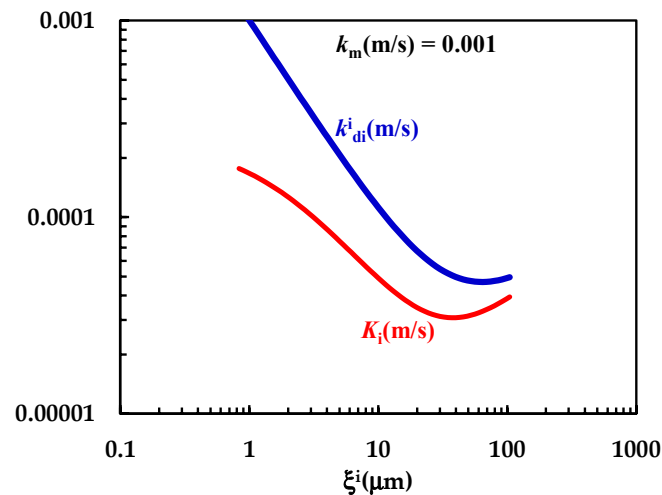


Figure 7. Comparison between k_m and the $k_d^i - K_i$ trend referring to the interpretation of DRT data (PRQ) according to the proposed mathematical model.

4.2.3. Comparison Between Drugs

The analysis of DRT data by means of the proposed mathematical model is confirmed by the results of drugs surface characterization, summarized in Figure 8. Indeed, for PRQ, drug wettability decreases with fluid polarity (solid line), as can be observed from the progressive decrease in the spreading coefficient (S_c , Equation (1)) with fluid polarity. Remarkably, S_c variation between water and diiodomethane is considerable, (around 50 mJ/m^2). On the other hand, for TPH, wettability reaches a maximum when fluid polarity is between 20 and 30% (S_c zeroes), while it decreases for higher and lower polarities (dashed line in Figure 8). In this case, S_c variation is about 25 mJ/m^2 , i.e., 50% of the that of PRQ. These considerations match with the TPH polarity feature, which is $\approx 51\%$ (an almost amphiphilic behavior; dashed vertical line in Figure 8), while PRQ's polarity is $\approx 25\%$ (a typical a-polar behavior; solid vertical line in Figure 8), i.e., one half of that of TPH. Thus, the lower PRQ polarity compared to that of TPH is perfectly compatible with the lower k_m value associated with PRQ with reference to that of TPH.

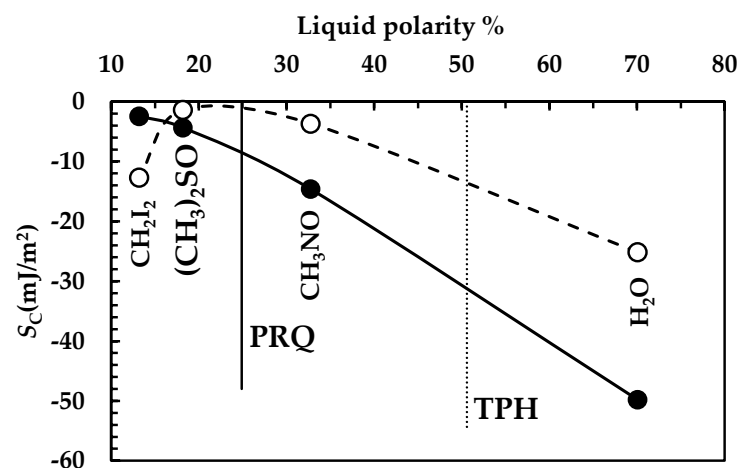


Figure 8. Spreading coefficient (S_c) referring to the four liquids considered (of increasing polarity, see Table 2) on PRQ (solid line) and TPH (dashed line). Vertical solid and dotted lines indicate, respectively, PRQ and TPH's polarities (see Table 3) (25°C).

However, the different dissolution behavior of TPH and PRQ is also due to different k_d^i (about one order of magnitude bigger in the TPH case, see Figures 5 and 7). This leads to a smaller BL average thickness in the TPH case ($\approx 0.1 \mu\text{m}$) with reference to PRQ ($\approx 3.7 \mu\text{m}$). The combination of surface wettability and BL thickness makes the resistance to drug

dissolution of PRQ about 35 times higher than that of TPH. Bearing in mind that PRQ solubility is about two orders of magnitude lower than that of TPH, PRQ dissolution is remarkably slow compared to that of TPH.

5. Conclusions

Despite the complexity of the mathematical model developed, we showed that the DRT data for both model drugs (theophylline and praziquantel) were successfully fitted by means of just two fitting parameters. In detail, the mentioned parameters are k_m , the mass transfer coefficient related to the first three steps of the dissolution process and mainly depending on the surface wettability, and α (see Equation (7)), which refers to the effect on dissolution of the relative velocity between particles and dissolution medium. Moreover, the presented mathematical model proposes as an elegant, user-friendly tool which can be run in a simple, yet effective, Microsoft Excel sheet as a user-defined function. Thus, data fitting was performed using the Solver functionality. Hence, the proposed mathematical model revealed two main outcomes as a result of the data interpretation in terms of micro- and macroscopic aspects. As concerns the microscopic aspects, we were able to determine how the relative importance of solid wettability and boundary layer, represented by the k_m/k_d ratio, affects the drug concentration profile inside the boundary layer during the entire dissolution process. As this time evolution cannot be experimentally detected, the proposed model behaved as a sort of theoretical microscope and allowed us to understand the missing insights into DRT. On the other hand, as concerns the macroscopic aspects, a comprehensive, robust strategy was proposed regarding the role of drug properties (mainly wettability and solubility), particle size distribution, and dissolution medium hydrodynamics on the DRT kinetics. Data fitting confirmed the importance of the different physical phenomena leading the dissolution of different poly-disperse solid drug particles. In particular, we found a perfect match between model outcomes in terms of k_m value and drug wettability evaluated through the spreading coefficient and the surface polarity. Hence, the mathematical model showed a reliable hallmark, able to evaluate the relative importance of the most pivotal phenomena involved in the DRT process, the key information required in experimental, industrial, and theoretical applications.

Author Contributions: Conceptualization, A.B., F.P., M.G., D.V. and M.A.; methodology, A.B., M.G., I.C. and D.V.; software, F.P., A.C., M.G., I.C. and L.G.; validation, A.B., F.P., G.M., E.F., L.G. and M.A.; formal analysis, F.P., A.C., L.G., I.C., M.G. and M.A.; investigation, A.B., F.P., G.M., E.F., A.C., L.G., D.V., I.C., G.G., M.G. and M.A.; data curation, A.B., F.P., G.M., E.F. and M.A.; writing—original draft preparation, M.G., G.M., E.F. and L.G.; writing—review and editing, A.B., F.P., G.M., E.F., A.C., L.G., D.V., I.C., G.G., M.G. and M.A.; visualization, L.G.; supervision, A.B., G.M., A.C., D.V., I.C., G.G., M.G. and M.A. All authors have read and agreed to the published version of the manuscript.

Funding: This research has received funding from the European Union-NextGenerationEU through the Italian Ministry of University and Research under NRRP-M4C2-I1.3 Project PE_00000019: “Health Extended ALLiance for Innovative Therapies, Advanced Lab-research, and Integrated Approaches of Precision Medicine-HEAL ITALIA” to G.M., CUP: B73C22001250006 of University of Palermo. The research leading to these results has also received funding from the European Union-NextGenerationEU through the Italian Ministry of University and Research under NRRP-M4C2-I1.3 Project PE_00000019: “Health Extended ALLiance for Innovative Therapies, Advanced Lab-research, and Integrated Approaches of Precision Medicine-HEAL ITALIA” to G.M., CUP: E93C22001860006 of University of Modena and Reggio Emilia. The views and opinions expressed are those of the authors only and do not necessarily reflect those of the European Union or the European Commission. Neither the European Union nor the European Commission can be held responsible for them.

Institutional Review Board Statement: Not applicable.

Informed Consent Statement: Not applicable.

Data Availability Statement: All the presented data are available upon request to the corresponding author.

Conflicts of Interest: The authors declare no conflicts of interest.

Appendix A

Figures A1 and A2 show the UV calibration curves referring to TPH and PRQ, respectively.

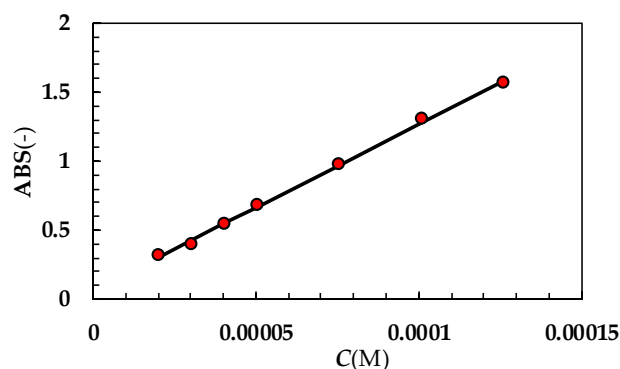


Figure A1. UV calibration curve referring to TPH (optical path = 1 cm; 37 °C). While ABS is absorbance, C is concentration expressed in moles/liter. Red dots indicate experimental data while the solid line is the linear interpolant ($ABS = (12,117 \pm 277) \times C + (0.05 \pm 0.022)$; Pearson correlation coefficient = 0.999). Molar extinction $\epsilon(M^{-1} \times cm^{-1}) = (12,117 \pm 227)$.

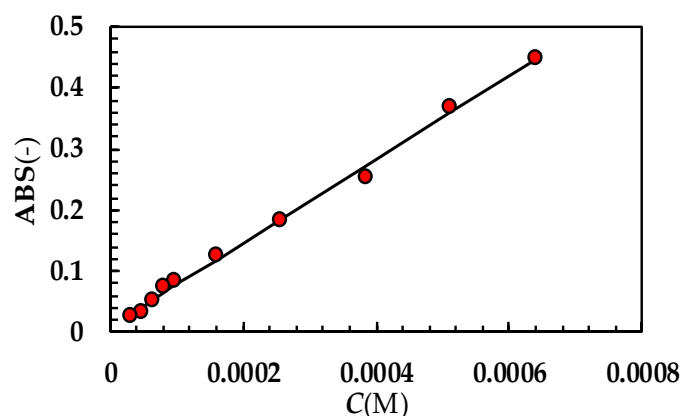


Figure A2. UV calibration curve referring to PRQ (optical path 2 cm; 37 °C). While ABS is absorbance, C is concentration expressed in moles/liter. Red dots indicate experimental data while the solid line is the linear interpolant ($ABS = (685 \pm 15) \times C + (0.01 \pm 0.005)$; Pearson correlation coefficient = 0.998). Molar extinction $\epsilon(M^{-1} \times cm^{-1}) = (342.3 \pm 7.5)$.

Appendix B

The numerical method adopted to solve model equations is depicted in Figure A3. At the beginning ($t = 0$) of the DRT process (**step 0**), the dissolution environment does not contain either the dissolved drug ($C_b = 0$) or the recrystallized drug ($M_c = 0$). Obviously, the radius of each of the N ($=50$) particles classes equates its own initial value $\zeta_{\min-0}^i$. **Step 1** aims to evaluate, at time ($t + \Delta t$; $\Delta t = 1s$), the particles' radii (ζ_{\min}^i), solving, by means of the Euler implicit method, the N ordinary differential equations ruling the time variation of each ζ_{\min}^i . Should the new ζ_{\min}^i evaluation be less than zero (**step 2**), ζ_{\min}^i is set to zero. **Step 3** serves to estimate the drug concentration in the dissolution environment (C_b) by means of a global mass balance. Indeed, it is essential to know whether C_b is lower than drug solubility (C_s) or not (**step 4** the question mark refers to the question: "is C_b lower than solubility C_s ?"). If $C_b > C_s$ (**step 5**), dissolution is stopped and the overall mass transport coefficients (K_i) are set to zero.

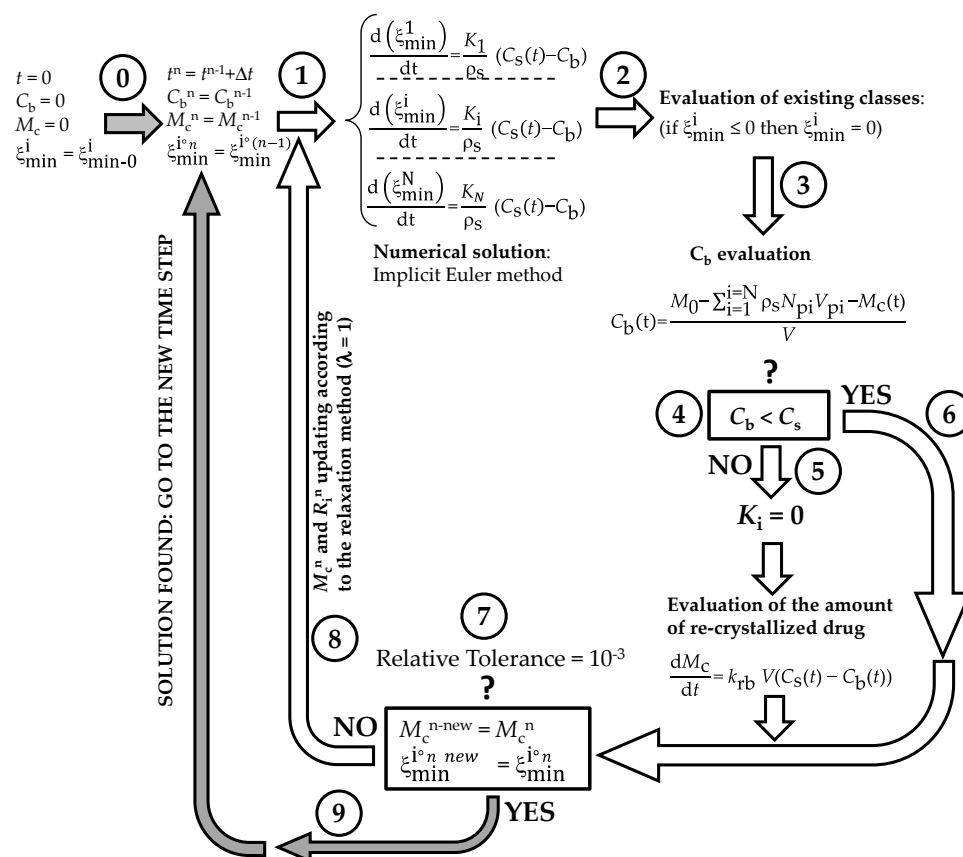


Figure A3. Schematic representation of the iterative method adopted to numerically solve the proposed mathematical model.

Contemporarily, the increase in the recrystallized drug amount (M_c) is evaluated by solving (implicit Euler method) the pertinent ordinary differential equation. Then, the algorithm proceeds to the convergence check (**step 7**: the question mark refers to the convergency question: “is the difference between the old and the new evaluations of particles radii lower than the relative tolerance?”) as occurs when $C_b < C_s$ (**step 6**). At **step 7**, the new evaluations of particles’ radii ($\xi_{\min}^{n-\text{new}}$) and re-crystallized drug amount ($M_c^{n-\text{new}}$) are compared to their last known values. If the difference between new and old values is less than tolerance (10^{-3}), the algorithm records all the calculated values and proceeds towards the new time step (grey arrow; **step 9**). On the contrary, a new iteration begins (**step 8**, white arrow) and variable values are updated according to the relaxation method. The procedure continues up to convergence.

In order to determine the unknown model parameters (k_m and α), the solution algorithm was embedded in a Microsoft Excel user-defined function. In doing so, we could take advantage of the “Solver” function that enabled us to easily fit the mathematical model to the experimental DRT data.

References

- Laitinen, R.; Lahtinen, J.; Silfsten, P.; Vartiainen, E.; Jarho, P.; Ketolainen, J. An optical method for continuous monitoring of the dissolution rate of pharmaceutical powders. *J. Pharm. Biomed. Anal.* **2010**, *52*, 181–189. [[CrossRef](#)] [[PubMed](#)]
- Stukelj, J.; Agopov, M.; Yliruusi, J.; Stachan, C.J. Image-based dissolution analysis for tracking the surface stability of amorphous powders. *ADMET DMPK* **2020**, *8*, 401–409. [[CrossRef](#)] [[PubMed](#)]
- Kwan, K.C. Oral bioavailability and first pass effects. *Drug Metab. Dispos.* **1997**, *25*, 1329–1336. [[PubMed](#)]
- Naidu, R.; Semple, K.T.; Megharaj, M.; Juhasz, A.L.; Bolan, N.S.; Gupta, S.K.; Clothier, B.E.; Schulin, R. Bioavailability: Definition, assessment and implications for risk assessment. *Dev. Soil Sci.* **2008**, *32*, 39–51. [[CrossRef](#)]
- Loftsson, T.; Brewster, M.E. Pharmaceutical applications of cyclodextrins: Basic science and product development. *J. Pharm. Pharmacol.* **2010**, *62*, 1607–1621. [[CrossRef](#)]

6. Davis, M.; Walker, G. Recent strategies in spray drying for the enhanced bioavailability of poorly water-soluble drugs. *J. Contr. Rel.* **2018**, *269*, 110–127. [[CrossRef](#)]
7. Gigliobianco, M.R.; Casadidio, C.; Censi, R.; Di Martino, P. Nanocrystals of Poorly Soluble Drugs: Drug Bioavailability and Physicochemical Stability. *Pharmaceutics* **2018**, *10*, 134. [[CrossRef](#)]
8. Bertoni, S.; Albertini, B.; Passerini, N. Spray Congealing: An Emerging Technology to Prepare Solid Dispersions with Enhanced Oral Bioavailability of Poorly Water Soluble Drugs. *Molecules* **2019**, *24*, 3471. [[CrossRef](#)]
9. Hixson, W.; Crowell, J.H. Dependence of reaction velocity upon surface and agitation I. Theoretical consideration. *Ind. Eng. Chem.* **1931**, *23*, 923–931. [[CrossRef](#)]
10. Hixson, W.; Crowell, J.H. Dependence of reaction velocity upon surface and agitation II. Experimental procedure in study surface. *Ind. Eng. Chem.* **1931**, *23*, 1002–1009. [[CrossRef](#)]
11. Hixson, W.; Crowell, J.H. Dependence of reaction velocity upon surface and agitation III. Experimental procedure in study of agitation. *Ind. Eng. Chem.* **1931**, *23*, 1160–1169. [[CrossRef](#)]
12. Niebergall, P.J.; Milosovich, G. Dissolution of particles under conditions of rapid agitation. *J. Pharm. Sci.* **1963**, *52*, 236–241. [[CrossRef](#)] [[PubMed](#)]
13. Pedersen, V.P.; Brown, K.F. Dissolution profile in relation to initial particle distribution. *J. Pharm. Sci.* **1975**, *64*, 1192–1195. [[CrossRef](#)] [[PubMed](#)]
14. Pedersen, V.P.; Brown, K.F. Size distribution effects in multiparticulate dissolution. *J. Pharm. Sci.* **1975**, *64*, 1981–1986. [[CrossRef](#)]
15. Pedersen, V.P.; Brown, K.F. General class of multiparticulate dissolution models. *J. Pharm. Sci.* **1977**, *66*, 1435–1438. [[CrossRef](#)]
16. Pedersen, V.P.; Myrick, J.W. Versatile kinetic approach to analysis of dissolution data. *J. Pharm. Sci.* **1978**, *67*, 1450–1455. [[CrossRef](#)]
17. Hsu, J.P.; Liu, B.T. Dissolution of solid particles in liquids: A reaction-diffusion model. *Colloids Surf.* **1993**, *69*, 229–238. [[CrossRef](#)]
18. Grassi, M.; Grassi, G.; Lapasin, R.; Colombo, I. *Understanding Drug Release and Absorption Mechanisms: A Physical and Mathematical Approach*; CRC Press: Boca Raton, FL, USA, 2007.
19. Guo, N.; Hou, B.; Wang, N.; Xiao, Y.; Hiang, J.; Guo, Y.; Zong, S.; Hao, H. In situ monitoring and modeling of the solution-mediated polymorphic transformation of rifampicin: From form II to form I. *J. Pharm. Sci.* **2018**, *107*, 344–352. [[CrossRef](#)]
20. Abrami, M.; Grassi, L.; di Vittorio, R.; Hasa, D.; Perissutti, B.; Voinovich, D.; Grassi, G.; Colombo, I.; Grassi, M. Dissolution of an ensemble of differently shaped poly-dispersed drug particles undergoing solubility reduction: Mathematical modelling. *ADMET DMPK* **2020**, *8*, 297–313. [[CrossRef](#)]
21. Thormann, D.U.; De Mieri, M.; Neuburger, M.; Verjee, S.; Altmann, P.; Hamburger, M.; Imanidis, G. Mechanism of chemical degradation and determination of solubility by kinetic modeling of the highly unstable sesquiterpene lactone nobilin in different media. *J. Pharm. Sci.* **2014**, *103*, 3139–3152. [[CrossRef](#)]
22. Mosharraf, M.; Nyström, C. The effect of particle size and shape on the surface specific dissolution rate of micronized practically insoluble drugs. *Int. J. Pharm.* **1995**, *122*, 35–47. [[CrossRef](#)]
23. Hirai, D.; Iwao, Y.; Kimura, S.I.; Noguchi, S.; Itai, S. Mathematical model to analyze the dissolution behaviour of metastable crystals or amorphous drug accompanied with solid-liquid interface reaction. *Int. J. Pharm.* **2017**, *522*, 58–65. [[CrossRef](#)] [[PubMed](#)]
24. Hsu, S.-Y.; Wu, C.-W. Effects of particle shape in mass-diffusion-controlled dissolution process. *Int. Comm. Heat Mass Transf.* **2021**, *125*, 105321. [[CrossRef](#)]
25. Yuan, Q.; Jia, X.; Williams, R.A. Validation of a multi-component digital dissolution model for irregular particles. *Powder Technol.* **2013**, *240*, 25–30. [[CrossRef](#)]
26. Hsu, J.P.; Lin, D.L.; Lin, M.J. Dissolution of solid particles in liquids: A surface layer model. *Colloids Surf.* **1991**, *61*, 35–47. [[CrossRef](#)]
27. Wang, J.; Flanagan, D.R. General solution for diffusion controlled dissolution of spherical particles 1. Theory. *J. Pharm. Sci.* **1999**, *88*, 731–738. [[CrossRef](#)]
28. Hasa, D.; Perissutti, B.; Voinovich, D.; Abrami, M.; Farra, R.; Fiorentino, S.M.; Grassi, G.; Grassi, M. Drug Nanocrystals: Theoretical Background of Solubility Increase and Dissolution Rate Enhancement. *Chem. Biochem. Eng. Q.* **2014**, *28*, 247–258. [[CrossRef](#)]
29. Salish, K.; So, C.; Jeong, S.H.; Hou, H.H.; Mao, C. A Refined Thin-Film Model for Drug Dissolution Considering Radial Diffusion-Simulating Powder Dissolution. *Pharm. Res.* **2024**, *41*, 947–958. [[CrossRef](#)]
30. D’Arcy, D.M.; Persoons, T. Mechanistic Modelling and Mechanistic Monitoring: Simulation and Shadowgraph Imaging of Particulate Dissolution in the Flow-Through Apparatus. *J. Pharm. Sci.* **2011**, *100*, 1102–1115. [[CrossRef](#)]
31. D’Arcy, D.M.; Persoons, T. Understanding the Potential for Dissolution Simulation to Explore the Effects of Medium Viscosity on Particulate Dissolution. *AAPS PharmSciTech* **2019**, *20*, 47. [[CrossRef](#)]
32. Abrami, M.; Grassi, M.; Masiello, D.; Pontrelli, G. Dissolution of irregularly-shaped drug particles: Mathematical modelling. *Europ. J. Pharm. Biopharm.* **2022**, *177*, 199–210. [[CrossRef](#)] [[PubMed](#)]
33. Grassi, M.; Colombo, I.; Lapasin, R. Experimental determination of the theophylline diffusion coefficient in swollen sodium-alginate membranes. *J. Contr. Rel.* **2001**, *76*, 93–105. [[CrossRef](#)] [[PubMed](#)]
34. Zanolli, D.; Perissutti, B.; Passerini, N.; Chierotti, M.R.; Hasa, D.; Voinovich, D.; Gigli, L.; Demitri, N.; Geremia, S.; Keiser, J.; et al. A new soluble and bioactive polymorph of praziquantel. *Eur. J. Pharm. Biopharm.* **2018**, *127*, 19–28. [[CrossRef](#)] [[PubMed](#)]
35. Biasin, A.; Pribac, F.; Milcovich, G.; Franceschinis, E.; Hasa, D.; Voinovich, D.; Grassi, G.; Grassi, M.; Abrami, M. Wettability and hydrodynamics key hallmarks on drugs’ dissolution rate. In Proceedings of the XXIII Simposio ADRITELF, Trieste, Italy, 11–13 September 2023; Poster 46. p. 155.

36. Grüßer, M.; Waugh, D.G.; Lawrence, J.; Langer, N.; Scholz, D. On the Droplet Size and Application of Wettability Analysis for the Development of Ink and Printing Substrates. *Langmuir* **2019**, *35*, 12356–12365. [[CrossRef](#)]
37. Bergese, P.; Colombo, I.; Federici, S. Thermodynamics of (nano)interfaces. In *Colloidal Foundations of Nanoscience*, 2nd ed.; Berti, D., Palazzo, G., Eds.; Elsevier: Amsterdam, The Netherlands, 2022; pp. 12–56.
38. Wu, S.J. Calculation of interfacial tension in polymer systems. *Polym. Sci. C* **1971**, *34*, 19–30. [[CrossRef](#)]
39. Kwok, D.Y.; Neumann, A.W. Contact angle measurement and contact angle interpretation. *Adv. Colloid Interface Sci.* **1999**, *81*, 167–249. [[CrossRef](#)]
40. Kwok, D.Y.; Neumann, A.W. Contact angle interpretation in terms of solid surface tension. *Colloids Surf. A Physicochem. Eng. Asp.* **2000**, *161*, 31–48. [[CrossRef](#)]
41. de Boer, G.B.J.; de Weerd, C.; Thoenes, D.; Goossens, H.W.J. Laser Diffraction Spectrometry: Fraunhofer Diffraction Versus Mie Scattering. *Part. Charact.* **1987**, *4*, 14–15. [[CrossRef](#)]
42. Tenchov, B.G.; Yanev, T.K. Weibull distribution of particle sizes obtained by uniform random fragmentation. *J. Colloid Interface Sci.* **1986**, *111*, 1–7. [[CrossRef](#)]
43. Nogami, H.; Nagai, T.; Yotsuyanagi, T. Dissolution phenomena of organic medicinals involving simultaneous phase changes. *Chem. Pharm. Bull.* **1969**, *17*, 499–509. [[CrossRef](#)]
44. Chiarappa, G.; Piccolo, A.; Colombo, I.; Hasa, D.; Voinovich, D.; Moneghini, M.; Grassi, G.; Farra, R.; Abrami, M.P.; Posocco, P.; et al. Exploring the Shape Influence on Melting Temperature, Enthalpy, and Solubility of Organic Drug Nanocrystals by a Thermodynamic Model. *Cryst. Growth Des.* **2017**, *17*, 4072–4083. [[CrossRef](#)]

Disclaimer/Publisher’s Note: The statements, opinions and data contained in all publications are solely those of the individual author(s) and contributor(s) and not of MDPI and/or the editor(s). MDPI and/or the editor(s) disclaim responsibility for any injury to people or property resulting from any ideas, methods, instructions or products referred to in the content.